RESEARCH PAPER

Molecular Modelling And Computational Evaluation Of Functionalised Isoxazoline As Novel Mao Inhibitors For Parkinson'S Disease

Zakiya Fathima C[1], Jainey P James[2*], Sindhu T.J[3]

[1,2,3] Nitte (Deemed To Be University), Ngsm Institute Of Pharmaceutical Sciences (Ngsmips), Department Of Pharmaceutical Chemistry, Mangalore-575018, Karnataka, India.

Corresponding Author: Dr. Jainey P. James, Associate Professor, Department Of Pharmaceutical Chemistry, Ngsm Institute Of Pharmaceutical Sciences (Ngsmips), Nitte (Deemed To Be University), Paneer, Deralakatte, Mangalore -575018, Karnataka, India. Email: jaineyjames@gmail.com

Received: *20th Feb, 2026;* ***Revised:*** *4th Mar, 2026;* ***Accepted:*** *25th Mar, 2026;* ***Available Online:*** *10th Apr, 2026*

Abstract

Parkinsons disease (pd), is a multifactorial neurodegenerative disorder characterised by progressive dopaminergic neuronal degeneration. A series of functionalised isoxazoline derivatives (4a–4h and 7a–7h) were designed and evaluated for their potential as monoamine oxidase-b (mao-b) inhibitors through comprehensive in silico studies, including physicochemical property assessment, drug-likeness profiling, adme prediction, toxicity risk evaluation, molecular docking, mm-gbsa binding free energy analysis, receptor-based pharmacophore modelling, and pass prediction.

All compounds exhibited favourable physicochemical profiles, complying with druglikeness rules with a consistent bioavailability score of 0.55. Pharmacokinetic profile and effective blood-brain barrier penetration. Toxicity assessment indicated a safe profile for most derivatives, except for 4h and 7h.

Molecular docking against mao-b (pdb id: 2byb) demonstrated strong binding affinities, with compounds 7b (−10.51 kcal/mol), 7e (−10.32 kcal/mol), and 4g (−10.29 kcal/mol) outperforming the reference drug deprenyl (−6.46 kcal/mol). These compounds exhibited key hydrogen bonding interactions along with extensive hydrophobic and pi-pi stacking interactions. Mmgbsa analysis further confirmed binding stability, with compound 7b showing the lowest binding free energy (−58.55 kcal/mol), primarily driven by van der waals and lipophilic contributions. Pharmacophore modelling revealed essential features such as hydrogen bond acceptors, hydrophobic regions, and aromatic interactions, with 7b showing optimal alignment within the active site. Pass prediction supported mao-related activity, particularly for the 7-series, while promiscuity and pains analysis confirmed low off-target risk and good synthetic accessibility.

Collectively, compound 7b emerged as the most promising lead candidate; further in vitro and in vivo studies were warranted to establish its therapeutic potential in pd.

Keywords: Parkinson'S Disease, Isoxazoline, Mao-B, Molecular Docking, Mmgbsa, Pharmacophore Modelling, Admet.

How To Cite This Article: Zakiya Fathima C, Jainey P James, Sindhu Tj. Molecular Modelling And Computational Evaluation Of Functionalised Isoxazoline As Novel Mao Inhibitors For Parkinson'S Disease. Int J Drug Deliv Technol. 2026;16(26s):281-295. Doi: 10.25258/ijddt.16.26s.29

INTRODUCTION

Parkinson's disease (PD) is a progressive neurodegenerative disorder characterised by the selective degeneration of dopaminergic neurons in the substantia nigra pars compacta, leading to motor impairments such as tremors, rigidity, bradykinesia, and postural instability [1,2]. The pathogenesis of PD is multifactorial, involving oxidative stress, mitochondrial dysfunction, neuroinflammation, and abnormal protein aggregation. Among these, the oxidative metabolism of dopamine plays a pivotal role in exacerbating neuronal damage by generating reactive oxygen species (ROS)[3,4].

Monoamine oxidases (MAOs), flavin-containing enzymes located on the outer mitochondrial membrane, are key regulators of monoamine neurotransmitter metabolism[5]. Two isoforms, MAO-A and MAO-B, are responsible for the oxidative deamination of biogenic amines. Notably, MAO-B predominates in the human brain and is significantly

upregulated with ageing and in PD. The enzymatic degradation of dopamine by MAO-B produces hydrogen peroxide and other toxic metabolites, contributing to oxidative stress and neurodegeneration. Consequently, inhibition of MAO, particularly MAO-B, has emerged as a well-established therapeutic strategy for PD management, as it enhances dopamine availability and mitigates oxidative damage[6].

Nitrogen-containing heterocyclic compounds represent a privileged class of molecules in medicinal chemistry due to their structural diversity, synthetic versatility, and ability to participate in key interactions with biological targets[7]. The presence of nitrogen atoms within heterocyclic frameworks facilitates hydrogen bonding, pi-pi stacking, and coordination with enzyme active sites, thereby enhancing binding affinity and selectivity. Several clinically approved MAO inhibitors, such as selegiline and rasagiline, incorporate nitrogen-containing heterocyclic moieties, underscoring their pharmacological relevance. Isoxazoline is a five-membered heterocyclic compound containing nitrogen and oxygen in its structure. These multiple heteroatoms contribute to a favourable electronic distribution and metabolic stability[8].

In recent years, considerable attention has been directed toward the design and development of novel nitrogen-containing heterocycles as potential MAO inhibitors. These compounds offer opportunities for structural optimisation to improve selectivity toward MAO-B, reduce adverse effects, and enhance pharmacokinetic properties. Computational approaches, including molecular docking, pharmacophore modelling, and molecular dynamics simulations, have become indispensable tools in accelerating the discovery of such candidates by providing insights into ligand enzyme interactions and structure-activity relationships[9].

In this context, the present study focuses on the computational evaluation of nitrogen-containing heterocyclic compounds as potential MAO inhibitors for the treatment of PD. By integrating *in silico* techniques, this work aims to identify promising scaffolds with enhanced binding affinity and favourable interaction profiles, thereby contributing to the rational design of effective neuroprotective agents.

MATERIALS AND METHODS

In silico study

Computational platform

All computational investigations were performed using the Maestro interface (version 13.9.138; Schrödinger Release 2024-1, Schrödinger, LLC, New York, USA) on a Linux x86_64 workstation. The system was configured with an Intel Core i7 octa-core processor, 16 GB RAM, and a 1 TB storage capacity, operating on a 64-bit architecture to ensure computational efficiency and stability.

Physicochemical and pharmacokinetic Profiling

The physicochemical characteristics, drug-likeness, and ADME (Absorption, Distribution, metabolism and excretion) properties of the designed compounds were systematically evaluated using the QikProp module (Schrödinger Suite 2024-1) and SwissADME. This *in silico* ADME assessment plays a crucial role in early-stage drug discovery by predicting ADME parameters, thereby minimising the likelihood of late-stage attrition. Furthermore, these descriptors provide critical insights into the compounds' bioavailability, safety profile, and overall druggability[10].

Toxicity Prediction

Toxicological profiling of the designed ligands was conducted using the OSIRIS Property Explorer. Evaluation of toxicity risks, including mutagenicity, tumorigenicity, irritancy, and reproductive effects, is essential for assessing the safety of novel chemical entities and facilitating their progression toward clinical development[11].

Ligand Preparation

The chemical structures of the designed ligands were initially sketched using ChemDraw and subsequently converted into SMILES notation for compatibility with the Maestro platform (Table 1). Ligand preparation was carried out using the LigPrep module, wherein three-dimensional geometries were generated under physiological conditions (pH 7.0 ± 2.0). The OPLS4 force field was employed for geometry optimisation and energy minimisation, ensuring the generation of low-energy, stereochemically accurate conformations suitable for molecular docking studies[12].

Table 1. The structure and SMILES of the designed ligands

Code	Structure	SMILES
4a	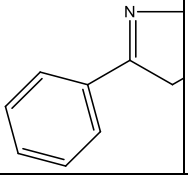	C1(C2=CC=CC=C2)=NOC(C1)C3=CC=CC=N3
4b	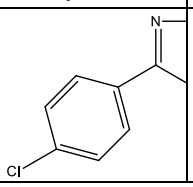	ClC1=CC=C(C2=NOC(C2)C3=CC=CC=N3)C=C1

4c	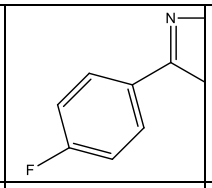	FC1=CC=C(C2=NOC(C2)C3=CC=CC=N3)C=C1
4d	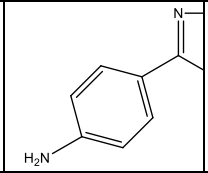	NC1=CC=C(C2=NOC(C2)C3=CC=CC=N3)C=C1
4e	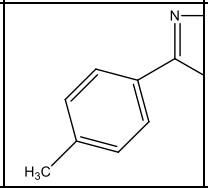	CC1=CC=C(C2=NOC(C2)C3=CC=CC=N3)C=C1
4f	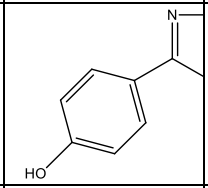	OC1=CC=C(C2=NOC(C2)C3=CC=CC=N3)C=C1
4g	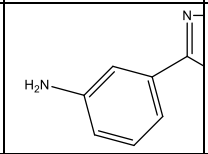	NC1=CC(C2=NOC(C2)C3=CC=CC=N3)=CC=C1
4h	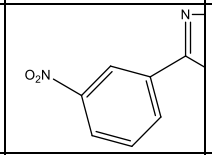	O=[N+]([O])C1=CC(C2=NOC(C2)C3=CC=CC=N3)=CC=C1
7a	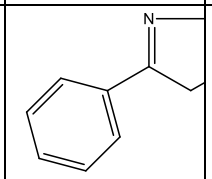	C1(C2=CC=CC=C2)=NOC(C1)C3=CC=NC=C3
7b	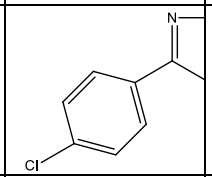	ClC1=CC=C(C2=NOC(C2)C3=CC=NC=C3)C=C1
7c	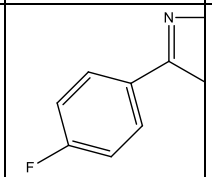	FC1=CC=C(C2=NOC(C2)C3=CC=NC=C3)C=C1
7d	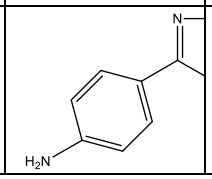	NC1=CC=C(C2=NOC(C2)C3=CC=NC=C3)C=C1
7e	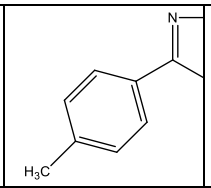	CC1=CC=C(C2=NOC(C2)C3=CC=NC=C3)C=C1
7f	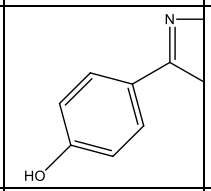	OC1=CC=C(C2=NOC(C2)C3=CC=NC=C3)C=C1
7g	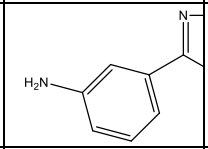	NC1=CC(C2=NOC(C2)C3=CC=NC=C3)=CC=C1
7h	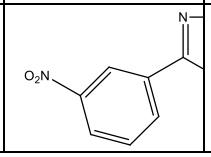	O=[N+]([O])C1=CC(C2=NOC(C2)C3=CC=NC=C3)=CC=C1

Target Protein Selection and Preparation

The crystal structure of monoamine oxidase (MAO) complexed with a reference ligand deprenyl (PDB ID: 2BYB) was retrieved from the RCSB Protein Data Bank. The selected structure, corresponding to *Homo sapiens*, exhibited a high-resolution value of 2.2 Å, ensuring structural reliability. Protein preparation was performed using the Protein Preparation Wizard in Maestro, which involved assignment of bond orders, addition of missing hydrogen atoms, optimisation of protonation states, and reconstruction of missing side chains and loops. Water molecules located beyond 5 Å from the active site were removed to avoid non-essential interactions. The prepared protein was subsequently subjected to restrained energy minimisation using the OPLS4 force field to achieve a stable and energetically favourable conformation[10,13].

Receptor Grid Generation

The receptor grid was generated using the Glide Grid Generation module to define the active site for docking. The grid box was centred on the co-crystallised ligand to accurately represent the binding pocket. The grid centre coordinates were set at X, Y, and Z axes, which were defined to ensure comprehensive coverage of the ligand-binding domain[14].

Molecular Docking

Molecular docking studies were performed using the Glide module in Extra Precision (XP) mode to predict the binding orientation and affinity of the designed ligands within the active site of MAO. The XP algorithm incorporates advanced scoring functions and flexible ligand sampling to enhance docking accuracy.

The optimal binding poses were selected based on the lowest Glide score in conjunction with favourable intermolecular interactions, including hydrogen bonding, pi-pi stacking, and hydrophobic contacts with key active site residues[15].

Binding Free Energy Calculations (Prime MM-GBSA)

The binding free energy (ΔG_bind) of the protein-ligand complexes was further evaluated using the Prime MM-GBSA approach. This method integrates molecular mechanics energies with implicit solvation models, accounting for both polar and non-polar contributions to solvation. The calculated ΔG_bind values (expressed in kcal/mol) provide a quantitative estimate of ligand binding affinity and stability of the complexes, thereby complementing docking results and enhancing the reliability of virtual screening outcomes[16].

Pharmacophore modelling

Pharmacophore modelling was performed using the Phase module implemented in the Schrödinger Suite. The receptor-based pharmacophore approach was employed to systematically identify and characterise the essential chemical features required for optimal ligand-target interactions. This method integrates structural information from the protein-ligand complex required for biological activity[17].

PASS (Prediction of Activity Spectra for Substances) prediction

The biological activity spectra of the designed compounds were predicted using the PASS (Prediction of Activity Spectra for Substances) online server. The molecular structures were initially constructed and subsequently converted into SMILES notation, which served as input for the PASS algorithm[18]. This computational approach employs a robust structure-activity relationship (SAR) based model to estimate the probability of a compound exhibiting a specific biological activity based on its structural features.

PAINS, promiscuity and synthetic accessibility assessment

Pan-assay interference compounds (PAINS) and compound promiscuity were systematically evaluated using the SwissADME and HitDexter 2.0 platforms to mitigate the risk of false-positive outcomes and ensure the identification of reliable and specific bioactive candidates. Further the synthetic accessibility was evaluated using SwissADME to evaluate its synthetic feasibility[19].

RESULTS AND DISCUSSION

Physicochemical properties

The physicochemical properties of the designed ligands (4a–4h and 7a–7h) were evaluated to determine their drug-likeness and suitability for central nervous system (CNS) activity and summarised in Table 2. All compounds exhibited molecular weights in the range of 224.26–269.26 Da, where within the acceptable limits of Lipinski's rule, indicating favourable oral bioavailability and permeability. The hydrogen bond donor (0.00–1.50) and acceptor (3.70–5.20) values were also within permissible ranges, suggesting a balanced polarity profile for membrane transport. The predicted lipophilicity (QPlog Po/w) ranged from 1.69 to 3.24, reflecting moderate lipophilicity optimal for CNS penetration[20]. Notably, compounds such as 4b and 4c demonstrated relatively higher lipophilicity, which may enhance passive diffusion across biological membranes, whereas compounds like 7d and 7g exhibited comparatively lower values, indicating increased polarity. The polar surface area (PSA) values ranged between 35.59 and 84.62 Å², with most compounds falling below the critical threshold of 70 Å², thereby suggesting good blood-brain barrier (BBB) permeability, although compounds 4h and 7h with higher PSA may exhibit comparatively reduced CNS penetration[21]. Furthermore, solvent accessible surface area (SASA) values (468.72–558.03 Å²) indicated moderate molecular exposure, while variations in hydrophobic (FOSA: 44.59–138.17 Å²) and hydrophilic (FISA: 47.61–189.11 Å²) surface areas highlighted differences in interaction potential and solubility among the compounds.

Table 2. Physicochemical properties of designed ligands

Ligands	Molwt	Donor HB	Accept HB	QPlog Po/w	#N and O	PSA	SASA	FOSA	FISA
4a	224.26	0.00	3.70	2.62	3.00	38.44	479.66	47.20	63.84
4b	258.71	0.00	3.70	3.24	3.00	35.59	504.25	53.68	50.69
4c	242.25	0.00	3.70	3.00	3.00	36.13	483.35	53.13	47.61

4d	239.28	1.50	4.70	1.97	4.00	62.69	495.18	50.22	119.19
4e	238.29	0.00	3.70	2.99	3.00	37.01	511.74	138.17	59.65
4f	240.26	1.00	4.45	2.11	4.00	60.83	495.92	50.74	119.02
4g	239.28	1.50	4.70	2.01	4.00	62.64	496.95	54.19	114.66
4h	269.26	0.00	4.70	1.95	6.00	81.48	520.51	50.92	154.56
7a	224.26	0.00	4.20	2.35	3.00	38.10	468.72	44.59	63.60
7b	258.71	0.00	4.20	2.86	3.00	38.15	493.52	44.70	63.82
7c	242.25	0.00	4.20	2.61	3.00	37.89	479.99	46.69	62.98
7d	239.28	1.50	5.20	1.69	4.00	63.67	492.34	49.87	127.49
7e	238.29	0.00	4.20	2.70	3.00	37.91	503.65	135.19	63.09
7f	240.26	1.00	4.95	1.87	4.00	60.52	481.62	44.97	117.97
7g	239.28	1.50	5.20	1.72	4.00	63.83	485.13	46.70	123.37
7h	269.26	0.00	5.20	1.78	6.00	84.62	558.03	45.83	189.11

Druglikeness of the designed ligands

The drug-likeness evaluation of the designed ligands as presented in Table 3, revealed that all compounds strictly comply with the major established drug-likeness filters, including Lipinski, Ghose, Veber, Egan, and Muegge criteria, with zero violations observed across all parameters. This uniform compliance indicates that the designed molecules possess optimal physicochemical attributes such as molecular weight, lipophilicity, hydrogen bonding capacity, and molecular flexibility, which are essential for favourable pharmacokinetic behaviour[22]. The absence of violations in these rules suggests good oral bioavailability, efficient membrane permeability, and an appropriate balance between hydrophilicity and lipophilicity. Furthermore, all compounds exhibited a consistent bioavailability score of 0.55, which is indicative of a high probability of adequate systemic absorption upon oral administration. This score is typically associated with compounds that meet key drug-likeness thresholds, further reinforcing their suitability as drug candidates.

Table 3. Druglikeness evaluation of designed ligands

Ligands	Lipinski	Ghose	Veber	Egan	Muegge	Bioavailability score
4a	0	0	0	0	0	0.55
4b	0	0	0	0	0	0.55
4c	0	0	0	0	0	0.55
4d	0	0	0	0	0	0.55
4e	0	0	0	0	0	0.55
4f	0	0	0	0	0	0.55
4g	0	0	0	0	0	0.55
4h	0	0	0	0	0	0.55
7a	0	0	0	0	0	0.55
7b	0	0	0	0	0	0.55
7c	0	0	0	0	0	0.55
7d	0	0	0	0	0	0.55
7e	0	0	0	0	0	0.55
7f	0	0	0	0	0	0.55
7g	0	0	0	0	0	0.55
7h	0	0	0	0	0	0.55

ADME profiling

The ADME profile of the designed ligands demonstrated favorable pharmacokinetic

characteristics (Table 4). The predicted human oral absorption (%HOA) was high for the majority of compounds, with several derivatives (4a–4c, 4e, 7a–7c, and 7e) exhibiting 100% absorption, indicating excellent oral bioavailability, while slightly reduced absorption was observed in more polar compounds such as 4h (83.64%) and 7h (76.78%). The Caco-2 (QPPCaco) and MDCK (QPPMDCK) permeability values, which are indicative of intestinal absorption and blood-brain barrier (BBB) permeability, respectively, were significantly high for most compounds, particularly 4b, 4c, and 7b, suggesting efficient membrane permeability and transport. In contrast, compounds such as 4h and 7h showed relatively lower permeability, likely due to increased polarity and higher polar surface area. The predicted brain/blood partition coefficient (QPlogBB) ranged from positive to moderately negative values, with compounds 4b, 4c, 7a–7c exhibiting favorable BBB penetration (QPlogBB > 0), whereas compounds like 4h and 7h showed poor CNS distribution (QPlogBB < -1), consistent with their CNS activity predictions[23]. The CNS activity scores further supported these findings, where compounds with values of 1 (4b, 4c, 7a–7c) are predicted to readily penetrate the CNS, while compounds such as 7h (-2) indicate negligible brain penetration (Figure 1). The number of predicted metabolic reactions (#metab) ranged from 4 to 6, suggesting moderate metabolic liability across the series, with slightly higher values in compounds 4g and 7g indicating increased susceptibility to biotransformation. Additionally, QPlogKhsa values, reflecting binding affinity to human serum albumin, were within acceptable limits (-1.5to 1.5), indicating balanced plasma protein binding without significant risk of bioaccumulation.

Table 4. ADME properties of designed ligands

Ligands	%HOA	QPPCaco	QPPMDCK	QPlogBB	CNS	#metab	QPlogKhsa
4a	100	2457.489	1307.45	-0.012	0	4	-0.084
4b	100	3274.751	4406.326	0.271	1	4	0.048
4c	100	3502.976	3469.493	0.257	1	4	-0.03
4d	89.752	733.939	354.115	-0.585	0	5	-0.079
4e	100	2692.797	1443.276	0.009	1	5	0.093
4f	90.635	736.596	355.501	-0.59	0	5	-0.039
4g	90.79	810.1	393.995	-0.548	0	6	-0.075
4h	83.642	338.982	153.648	-0.945	-1	5	-0.171
7a	100	2470.269	1314.801	0.013	1	4	-0.227
7b	100	2458.713	3227.751	0.171	1	4	-0.096
7c	100	2504.451	2415.559	0.125	1	4	-0.174
7d	86.74	612.225	291.089	-0.653	0	5	-0.164
7e	100	2498.382	1330.982	-0.005	0	5	-0.045
7f	89.396	753.762	364.464	-0.533	0	5	-0.141
7g	87.609	669.855	320.816	-0.585	0	6	-0.16
7h	76.786	159.438	67.99	-1.396	-2	5	-0.169

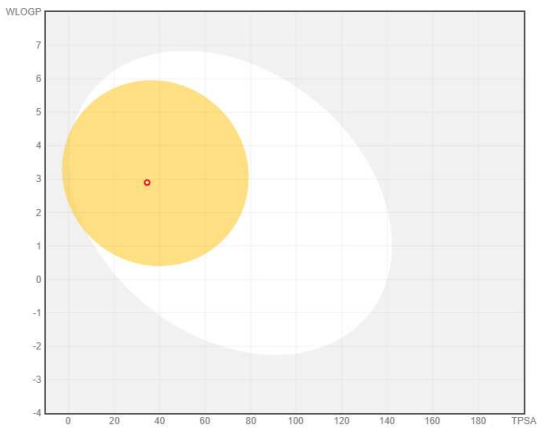

Figure 1. Predicted blood brain barrier (BBB) permeability of the 7b using the BOILED-Egg model

Predicted toxicity

The toxicity risk assessment of the designed ligands was presented in Table 5, revealing an overall favourable safety profile for the majority of compounds. Most derivatives demonstrated no predicted tumorigenic, mutagenic, irritant, or reproductive toxicity risks, indicating a high degree of chemical safety and suitability for further drug development. This suggests that the structural framework of these compounds is largely devoid of toxicophores commonly associated with adverse biological effects[24]. However, exceptions were observed for compounds 4h and 7h, which exhibited predicted tumorigenic and mutagenic risks, potentially attributable to specific structural features that may interact with genetic material or induce carcinogenic pathways. Importantly, none of the compounds showed irritant or reproductive toxicity risks, further supporting their biocompatibility. The absence of mutagenicity and tumorigenicity in the remaining compounds highlights their safer profile and strengthens their candidacy for therapeutic development. Collectively, these findings indicate that most of the designed ligands possess a favourable toxicity profile, with compounds excluding 4h and 7h emerging as promising and relatively safe candidates for further optimisation and preclinical evaluation in the context of Parkinson's disease.

Table 5. Toxicity and drug score profile of the designed ligands

Ligands	Tumorigenic	Mutagenic	Irritant	Reproductive risk
4a	No	No	No	No
4b	No	No	No	No
4c	No	No	No	No
4d	No	No	No	No
4e	No	No	No	No
4f	No	No	No	No
4g	No	No	No	No
4h	Yes	Yes	No	No
7a	No	No	No	No
7b	No	No	No	No
7c	No	No	No	No
7d	No	No	No	No
7e	No	No	No	No
7f	No	No	No	No
7g	No	No	No	No
7h	Yes	Yes	No	No

Molecular docking

The molecular docking analysis of the designed ligands against the target protein MAO (2BYB) revealed strong binding affinities and favourable interaction profiles when compared to the reference ligand, deprenyl. The docking scores ranged from -8.01 to -10.51 kcal/mol, indicating significantly higher binding affinity than deprenyl (-6.460 kcal/mol), thereby suggesting enhanced inhibitory potential of the synthesised compounds. Among the series, compounds 7b (-10.51 kcal/mol) (Figure 2), 7e (-10.32 kcal/mol) (Figure 3) and 4g (-10.29 kcal/mol) (Figure 4), exhibited the most favourable binding energies. The docking score and the interactions were summarised in Table 5.

Table 5. Docking score and interaction of the designed ligands with target 2BYB

Ligands	Docking score (kcal/mol)	H-bond	Polar interaction	Hydrophobic interaction	Pi-pi stacking
4a	-8.56	-	Gln 206	Trp 119, Leu 164, Phe 168, Ile 199, Ile 198, Leu 171, Cys 172, Tyr 398, Tyr 435, Phe 343, Tyr 326, Il3 316, Pro 104	-
4b	-8.28	-	Ser 59, Gln 206	Ile 316, Phe 343, Tyr 60, Tyr 435, Tyr 398, Tyr 326, Cys 172, Leu 171, Phe 168, Trp 119, Ile 199, Ile 198	Tyr 326, Phe 343

4c	-8.84	-	Gln 206	Tyr 326, Ile 199, Ile 198, Phe 343, Tyr 398, Tyr 435, Cys 172, Leu 171, Phe 168, Leu 167,Leu 164,Trp 119, Pro 104, Pro 102, Ile 316	-
4d	-8.44	Gly 434	Ser 59, Gln 206	Ile 198, Ile 199, Phe 168, Tyr 326, Leu 171, Cys 172, Tyr 188, Tyr 398, Tyr 435, Met 436, Tyr 60, Phe 343	Tyr 326, Tyr 435
4e	-8.60	-	Gln 206	Tyr 398, Tyr 60, Tyr 435, Phe 343, Tyr 326, Ile 316, Leu 164, Trp 119, Leu 167, Phe 168, Ile 199, Ile 198, Cys 172, Cys 171	-
4f	-8.49	-	Gln 206	Tyr 435, Tyr 60, Phe 343, Tyr 326, Ile 316, Pro 104, Leu 164, Trp 119, Leu 167, Phe 168, Leu 171, Cys 172, Ile 198, Ile 199	-
4g	-10.29	Gly 434, Tyr 188	Thr 399, Ser 59, Gln 206	Phe 168, Ile 199, Ile 198, Tyr 326, Leu 171, Cys 172, Tyr 188, Tyr 435, Tyr 398, Tyr 60, Phe 343	Tyr 326, Tyr 435
4h	-8.01	-	Gln 206	Ile 316, Ile 199, Ile 199, Phe 168, Tyr 326, Leu 171, Cys 172, Tyr 398, Tyr 188, Tyr 435, Phe 343, Tyr 60	Tyr 326, Tyr 398
7a	-8.35	Ser 59	Ser 59, Gln 206	Phe 168, Leu 171, Cys 172, Ile 198, Ile 199, Tyr 326, Tyr 398, Tyr 435, Met 436, Tyr 60, Phe 343	Tyr 326, Tyr 60
7b	-10.51	Ser 59, Tyr 60	Ser 59, Gln 206	Phe 168, Tyr 326, Leu 171, Cys 172, Ile 199, Ile 198, Tyr 398, Tyr 435, Met 436, Tyr 60, Phe 343	Tyr 60, Tyr 326

7c	-10.23	Ser 59	Ser 59, Gln 206	Phe 168, Leu 171, Cys 172, Ile 199, Ile 198, Tyr 398, Tyr 435, Met 436, Tyr 60, Phe 343, Tyr 326	Tyr 326, Tyr 60
7d	-8.72	Gly 434	Ser 59, Gln 206	Ile 199, Ile 198, Phe 168, Tyr 326, Leu 171, Cys 172, Tyr 188, Tyr 435, Tyr 398, Tyr 60, Phe 343	Tyr 326, Tyr 398
7e	-10.32	Ser 59	Ser 59, Gln 206	Phe 168, Tyr 326, Leu 171, Cys 172, Ile 199, Ile 198, Tyr 398, Tyr 435, Met 436, Tyr 60, Phe 343	Tyr 60, Tyr 326
7f	-10.00	Ser 59	Ser 59, Gln 206	Phe 168, Tyr326, Leu 171, Cys 172, Ile 199, Ile 198, Tyr 398, Tyr 435, Met 436, Tyr 60, Phe 343	Tyr 326, Tyr 60
7g	-9.97	Ser 59	Ser 59, Gln 206	Phe 168, Ile 199, Ile 198, Leu 171, Cys 172, Tyr 326, Tyr 398, Tyr 435, Met 436, Tyr 60, Phe 343	Tyr 60
7h	-9.79	Ser 59, Tyr 60	Ser 59, Gln 206	Cys 172, Leu 171, Phe 168, Ile 199, Ile 198, Tyr 326, Tyr 398, Tyr 435, Met 436, Tyr 60, Phe 343	Tyr 326, Tyr 60
Deprenyl	-6.460	-	Gln 206	Ile 198, Ile 199, Pro 104, Phe 103, Tyr 326, Tyr 398, Ile 316, Cys 172, Leu 171, Phe 168, Leu 167, Leu 164, Trp 119	-

Detailed interaction analysis demonstrated that polar interactions with key residues such as Gln 206 and Ser 59 were consistently observed across most of the ligands, indicating their crucial role in ligand stabilisation within the active site. Hydrogen bonding interactions, although not present in all compounds, were notably observed in 4g, 7b, 7c, 7e, 7f, 7g, and 7h (primarily with Ser 59 and Tyr 60), further contributing to binding specificity and stability. In contrast, hydrophobic interactions were extensively distributed across the active pocket, particularly involving residues such as Tyr 326, Tyr 398, Tyr 435, Phe 343, Phe 168, Ile 198, Ile 199, Leu 171, and Cys 172, which form a hydrophobic core essential for ligand accommodation.

Additionally, pi-pi stacking interactions were prominently observed in several high-affinity compounds, particularly involving aromatic residues Tyr 326, Tyr 60, and Phe 343, which are critical for

stabilising aromatic moieties of the ligands within the binding cavity. Compounds such as 7b, 7c, 7e, and 7f demonstrated consistent pi-pi interactions, correlating with their superior docking scores. Notably, the reference ligand deprenyl lacks both hydrogen bonding and pi-pi stacking interactions within the active site, which may account for its comparatively lower binding affinity; in contrast, the presence of these interactions in the designed ligands significantly enhances their binding stability and overall docking performance.

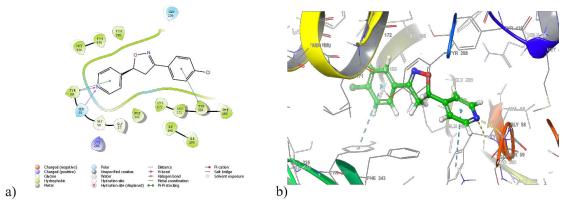

Figure 2. Molecular docking a) 2D b) 3D interaction of 7b with the active site of 2BYB

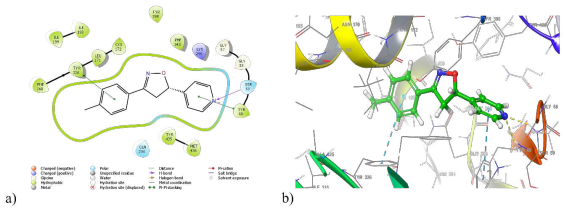

Figure 3. Molecular docking a) 2D b) 3D interaction of 7e with the active site of 2BYB

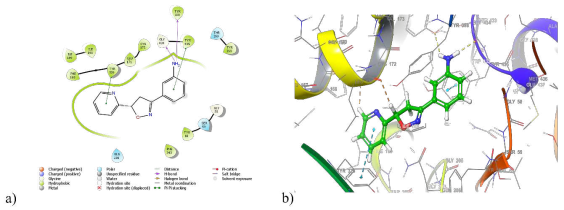

Figure 4. Molecular docking a) 2D b) 3D interaction of 5g with the active site of 2BYB

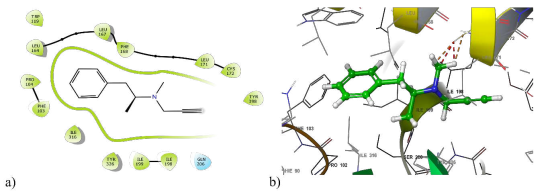

Figure 5. Molecular docking a) 2D b) 3D interaction of co-crystal (Deprenyl) with the active site of 2BYB

MMGBSA binding free energy

The MMGBSA binding free energy analysis of the designed ligands in complex with the target protein 2BYB provided deeper insights into the thermodynamic stability of the ligand protein interactions (Table 6). The total binding free energy (ΔG Bind) values ranged from −41.97 to −58.55 kcal/mol, with several compounds exhibiting more favourable binding energies than the reference ligand deprenyl (−50.35 kcal/mol). Notably, compounds 7b (−58.55 kcal/mol), demonstrated the most stable binding profiles, corroborating the docking results and reinforcing their potential as strong inhibitors.

Energy term contribution analysis revealed that van der Waals ((ΔG Bind vdW) and lipophilic (ΔG Bind Lipo) interactions were the major contributors to binding stability, with consistently high negative values across the series, indicating dominant hydrophobic interactions within the active site[25]. In contrast, coulombic contributions varied among the ligands, with some compounds such as 4f, 4g, 7d, and 7g, showing significantly favourable electrostatic interactions (high negative ΔG Coulomb values), enhancing overall binding affinity. The hydrogen bonding contribution (ΔG Bind H Bond) was relatively modest but supportive, aligning with the docking observations where selective hydrogen bond formation contributed to ligand stabilisation.

The solvation energy term (ΔG Bind Solv GB) was positive for most compounds, reflecting the energetic penalty associated with desolvation upon binding; however, this was effectively compensated by strong vdW and lipophilic interactions. Interestingly, the reference ligand deprenyl showed a comparatively less favourable vdW contribution (−28.85 kcal/mol) despite having a strong lipophilic component, which may partly explain its lower overall binding affinity compared to the designed ligands.

Table 6. MMGBSA binding free energy of the designed ligands with 2BYB

Ligands	ΔG Bind	ΔG Bind Coulomb	ΔG Bind Covalent	ΔG Bind H Bond	ΔG Bind Lipo	ΔG Bind Solv GB	ΔG Bind vdW
	kcal/mol						
4a	-49.15	-2.60	1.00	0.00	-26.93	-3.19	0.00
4b	-52.77	3.94	4.48	-0.01	-33.68	11.30	-38.30
4c	-	-2.03	1.14	-	-	17.	-

	45.37			0.00	26.59	93	35.24
4d	-53.51	-7.25	4.05	-0.22	-31.28	18.90	-37.31
4e	-41.97	3.87	6.43	0.00	-29.11	13.52	-36.49
4f	-56.47	-21.99	4.64	-0.57	-22.04	21.39	-37.20
4g	-55.17	-23.41	3.14	-1.78	-22.25	24.80	-34.98
4h	-53.57	13.06	3.62	-0.07	-23.48	-1.27	-44.53
7a	-48.24	-7.80	3.56	-0.22	-26.85	17.98	-34.46
7b	-58.55	-6.82	4.22	-0.23	-35.05	16.46	-36.68
7c	-49.88	-7.03	3.55	-0.22	-26.77	16.28	-35.25
7d	-53.69	-21.06	2.42	-1.76	-21.76	24.14	-35.00
7e	-56.47	-21.99	4.64	-0.57	-22.04	21.39	-37.20
7f	-47.18	-8.10	3.67	-0.23	-26.76	21.18	-36.51
7g	-54.06	-20.55	3.32	-1.13	-21.86	24.80	-37.78
7h	-54.37	9.47	0.09	-0.23	-27.08	4.39	-39.99
Deprenyl	-50.35	-0.01	2.26	0.00	-42.64	18.90	-28.85

Pharmacophore modelling

The receptor-based pharmacophore modelling of the top-docked compounds 7b and 7e in the active site of 2BYB (Figure 6) revealed key interaction features responsible for their high binding affinity and stability. The pharmacophore maps indicate that both compounds effectively align with critical binding features within the active pocket, including aromatic ring centers (R6), hydrophobic regions (H5 in 7b and H3 in 7e), and hydrogen bond acceptor (A1) functionalities. In both 7b (Figure 6a) and 7e (Figure 6b), the presence of aromatic moieties facilitates strong pi-pi interactions, with key residues such as Tyr 326 and Tyr 60, consistent with the docking results. Additionally, the identified hydrophobic interaction zones correspond well with residues like Phe 168, Leu 171, and Ile 199, indicating optimal hydrophobic packing within the binding cavity.

Furthermore, the pharmacophore model highlights the contribution of hydrogen bond acceptor features oriented toward polar residues such as Ser 59 in both 7b and 7e, supporting stable ligand anchoring. Notably, an additional hydrogen bond interaction between Tyr 60 and the pyridine nitrogen may further enhance binding stabilisation, thereby contributing to the comparatively higher binding affinity of these compounds among the designed derivativeshe distinct structural feature of 7b, the presence of a chloro substituent on the phenyl ring, was identified as a key hydrophobic feature (H4), which may be responsible for its increased lipophilicity and strengthened hydrophobic interactions within the binding cavity. This enhanced hydrophobic complementarity likely improves binding stability, thereby positioning 7b as the most promising candidate among the designed ligands.

The spatial arrangement of these features in both compounds demonstrates a high degree of complementarity with the receptor's active site geometry. Notably, compound 7b exhibits a more optimal alignment of pharmacophoric features, including better overlap with hydrophobic and aromatic regions, which may account for its superior docking score and MMGBSA binding energy compared to 7e.

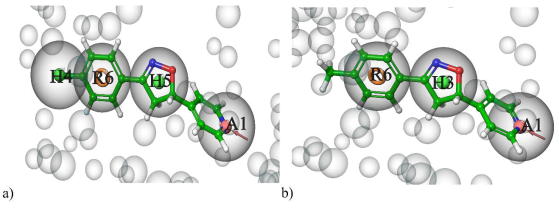

Figure 6. Receptor based pharmacophore modelling of a) 7b and b) 7e with the active site of 2BYB

PASS prediction

The PASS analysis for the designed ligands indicated varying probabilities for monoamine oxidase (MAO) reuptake inhibitory activity, as reflected by the Pa

(probability of activity) and Pi (probability of inactivity) values (Table 7). In general, compounds with Pa > Pi are considered more likely to exhibit the predicted biological activity[26]. Among the series, compounds 7b (Pa = 0.329, Pi = 0.045), demonstrated relatively higher Pa values along with low Pi values, suggesting a greater likelihood of MAO inhibitory potential. Compounds from the 4-series such as 4b (Pa = 0.269, Pi = 0.083) showed higher predicted activity, whereas compounds like 4e and 4f exhibited nearly comparable Pa and Pi values, indicating lower prediction confidence. Notably, several compounds (4c, 4d, and 4g) did not yield predicted activity for this endpoint, suggesting structural features less favorable for MAO inhibition.

Table 7. Predicted PASS activity as MAO reuptake inhibitor for the designed ligands

Ligands	Pa	Pi	Ligands	Pa	Pi
4a	0.233	0.112	7a	0.304	0.052
4b	0.269	0.083	7b	**0.329**	0.045
4c	-	-	7c	0.230	0.115
4d	-	-	7d	0.184	0.169
4e	0.220	0.215	7e	0.280	0.075
4f	0.185	0.167	7f	0.241	0.105
4g	-	-	7g	0.195	0.154
4h	0.224	0.121	7h	0.295	0.065

Predicted promiscuity, PAINS alert and synthetic accessibility of designed ligands

The evaluation of promiscuity, PAINS alerts, and synthetic accessibility for the designed ligands as presented in Table 8, provides important insights into their specificity and drug development feasibility. Most of the compounds were predicted to be non-promiscuous in both target-based and cell-based models, indicating a lower likelihood of off-target interactions and false-positive biological activity[27]. However, compounds 4d and 4e were identified as promiscuous in the target-based mode, suggesting a potential risk of non-specific binding that may require further experimental validation. Importantly, all compounds showed zero PAINS alerts, confirming the absence of pan-assay interference structures and supporting the reliability of their predicted biological activities. Furthermore, the synthetic accessibility (SA) scores ranged from 3.15 to 3.44, indicating that all compounds possess moderate to good synthetic feasibility.

Table 8. Predicted promiscuity, PAINS alert and synthetic accessibility of designed ligands

Ligands	Predicted confidence of a compound being promiscuous by		PAINS alert	Synthetic accessibility
4a	**Target-based mode**	**Extended cell-based mode**		
4b	Non-promiscuous compound	Non-promiscuous compound	0	3.33
4c	Non-promiscuous compound	Non-promiscuous compound	0	3.31
4d	Promiscuous compound	Non-promiscuous compound	0	3.3
4e	Promiscuous compound	Non-promiscuous compound	0	3.34
4f	Non-promiscuous compound	Non-promiscuous compound	0	3.42
4g	Non-promiscuous compound	Non-promiscuous compound	0	3.29
4h	Non-promiscuous compound	Non-promiscuous compound	0	3.37

7a	Non-promiscuous compound	Non-promiscuous compound	0	3.44
7b	Non-promiscuous compound	Non-promiscuous compound	0	3.18
7c	Non-promiscuous compound	Non-promiscuous compound	0	3.18
7d	Non-promiscuous compound	Non-promiscuous compound	0	3.16
7e	Non-promiscuous compound	Non-promiscuous compound	0	3.19
7f	Non-promiscuous compound	Non-promiscuous compound	0	3.27
7g	Non-promiscuous compound	Non-promiscuous compound	0	3.15
7h	Non-promiscuous compound	Non-promiscuous compound	0	3.23

CONCLUSION

The study revealed that designed compounds possess potent MAO-B inhibitory activity. The bioactivity is primarily governed by the presence of an aromatic scaffold enabling hydrophobic and pi-pi interactions, along with strategically positioned hydrogen bond acceptor groups such as the pyridine nitrogen. Halogen substitution, particularly chloro groups (7b), significantly enhances binding affinity by improving lipophilicity and hydrophobic interactions within the active site. In contrast, increased polarity or bulky substituents negatively impact CNS permeability and activity. The 7 series compounds (4-pyridine analogues) demonstrated superior activity over the 4 series (2-pyridine analogues), which can be attributed to the positional effect of the nitrogen atom within the pyridine ring. The 2-pyridine analogues may experience suboptimal orientation or steric constraints, limiting effective interaction with critical residues.

Overall, the study identifies the designed pyridine-isoxazoline scaffolds as potent candidates with significant MAO-B inhibitory potential. However, further *in vitro* and *in vivo* studies are necessary to validate these computational findings and to advance their potential application in PD therapy.

ACKNOWLEDGEMENT

The authors gratefully acknowledge NGSMIPS, the CADD Lab at NGSMIPS and Nitte (Deemed to be University).

DATA AVAILABILITY

The data that support the findings of this study are available from the corresponding author upon reasonable request.

CONFLICT OF INTEREST

The authors declare that no known financial or personal interests could have influenced the work reported in this study.

AUTHORSHIP CONTRIBUTION STATEMENT

Zakiya Fathima C: Hypothesis formulation, methodology, data compilation, interpretation, writing an original draft, **Janiney P James:** Conceptualisation, supervision, and validation, **Sindhu T.J:** Methodology, formal analysis and review and editing of the manuscript.

FUNDING INFORMATION

There is no funding information for this paper.

STATEMENT OF USAGE OF ARTIFICIAL INTELLIGENCE

Not received any help from artificial intelligence.

REFERENCES

1. Jankovic J, Tan EK. Parkinson's disease: etiopathogenesis and treatment. Journal of Neurology, Neurosurgery & Psychiatry. 2020;91(8):795-808. Doi:10.1136/jnnp-2019-322338
2. Kumar S, Goyal L, Singh S. Tremor and rigidity in patients with Parkinson's disease: emphasis on epidemiology, pathophysiology and contributing factors. CNS & Neurological Disorders-Drug Targets-CNS & Neurological Disorders). 2022;21(7):596-609. Doi:10.2174/1871527320666211006142100
3. Chakrabarti S, Bisaglia M. Oxidative stress and neuroinflammation in Parkinson's disease: the role of

dopamine oxidation products. Antioxidants. 2023;12(4):955. Doi:10.3390/antiox12040955

4. Huang M, Bargues-Carot A, Riaz Z, Wickham H, Zenitsky G, Jin H, Anantharam V, Kanthasamy A, Kanthasamy AG. Impact of environmental risk factors on mitochondrial dysfunction, neuroinflammation, protein misfolding, and oxidative stress in the etiopathogenesis of Parkinson's disease. International journal of molecular sciences. 2022;23(18):10808. Doi:10.3390/ijms231810808
5. Li B, An Z. Flavin-containing monooxygenases in the brain and their involvement in neurodegeneration and aging. Journal of Exploratory Research in Pharmacology. 2023;8(3):237-41. Doi:10.14218/JERP.2022.00067
6. Naoi M, Maruyama W, Shamoto-Nagai M, Riederer P. Type A monoamine oxidase; its unique role in mood, behavior and neurodegeneration. Journal of Neural Transmission. 2025;132(3):387-406. Doi: 10.1007/s00702-024-02866-z
7. Ebenezer O, Jordaan MA, Carena G, Bono T, Shapi M, Tuszynski JA. An overview of the biological evaluation of selected nitrogen-containing heterocycle medicinal chemistry compounds. International Journal of Molecular Sciences. 2022;23(15):8117. Doi: 10.3390/ijms23158117
8. Pandhurnekar CP, Pandhurnekar HC, Mungole AJ, Butoliya SS, Yadao BG. A review of recent synthetic strategies and biological activities of isoxazole. Journal of Heterocyclic Chemistry. 2023;60(4):537-65. DOI: https://doi.org/10.1002/jhet.4586
9. Ouma RB, Ngari SM, Kibet JK. A review of the current trends in computational approaches in drug design and metabolism. Discover Public Health. 2024;21(1):108. Doi:10.1186/s12982-024-00229-3
10. Fathima CZ, James PJ, Gatty V, Sindhu TJ, Sheqi A. Unveiling the Monoamine Oxidase Inhibitory Potential of Natural Flavonoids: A Computational Approach. Research Journal of Pharmacy and Technology. 2025;18(9):4289-96. Doi: 10.52711/0974-360X.2025.00616
11. Rajalakshmi R, Lalitha P, Sharma SC, Rajiv A, Chithambharan A, Ponnusamy A. In silico studies: Physicochemical properties, drug score, toxicity predictions and molecular docking of organosulphur compounds against Diabetes mellitus. Journal of Molecular Recognition. 2021;34(11):e2925.Doi: 10.1002/jmr.2925
12. Jouhara BM M, P. James J. Synthesis of Functionalized Isoxazolines as New Acetylcholinesterase and Tyrosinase Inhibitors and Antioxidant Agents. Polycyclic Aromatic Compounds. 2024;44(8):5294-313. Doi: 10.1080/10406638.2023.2264449
13. Fathima CZ, James JP, Dwivedi PS, Sindhu TJ. Molecular Docking, Pharmacophore Modeling, 3D QSAR, Molecular Dynamics Simulation and MMPBSA Studies on Hydrazine-Linked Thiazole Analogues as MAO-B Inhibitors. Journal of Computational Biophysics and Chemistry. 2025;24(06):709-32. Doi: 10.1142/S2737416524500790
14. TJ S, James JP, Fathima C Z, Dixit S, Kolachi KY. MD Simulations, DFT and Molecular Docking Studies of Schiff Base–Derived Heterocycles as Potent BuChE Inhibitors for Alzheimer's Disease. ChemistrySelect. 2026;11(1):e03914.Doi: 10.1002/slct.202503914
15. SRINIVASA MG. Investigating Multitarget Potential of Mucuna pruriens Against Parkinson's Disease: Insights From Molecular Docking, MMGBSA, Pharmacophore Modelling, MD Simulations and ADMET Analysis. International Journal of Applied Pharmaceutics. 2024;16(5), 176-193. Doi: 10.22159/ijap.2024v16i5.51474
16. TJ S, James JP, Zakiya Fathima C, Mathew B, Kumar S. Mechanistic Insights into Thiazolidinones as Anticholinesterase Agents: 3D QSAR Pharmacophore Modeling, Molecular Docking, MD Simulations, and DFT Studies for Alzheimer's Therapy. J. Comput. Biophys. Chem. 2025;24(10):1415-40. Doi:10.1142/S2737416525500309
17. Upadhyay RK. Drug delivery systems, CNS protection, and the blood brain barrier. BioMed research international. 2014;2014(1):869269. Doi: Upadhyay RK. Drug delivery systems, CNS protection, and the blood brain barrier. BioMed research international. 2014;2014(1):869269. Doi:Upadhyay RK. Drug delivery systems, CNS protection, and the blood brain barrier. BioMed research international. 2014;2014(1):869269. Doi: 10.3390/ijms17071087
18. Putz MV, Duda-Seiman C, Duda-Seiman D, Putz AM, Alexandrescu I, Mernea M, Avram S. Chemical structure-biological activity models for pharmacophores' 3D-interactions. International journal of molecular sciences. 2016;17(7):1087. Doi:
19. Shukla R, Tripathi T. Molecular dynamics simulation of protein and protein–ligand complexes. InComputer-aided drug design 2020 (pp. 133-161). Singapore: Springer Singapore. Doi:10.1007/978-981-15-6815-2_7
20. Ibrahim SO, Lukman HY, Zubair MF, Amusan OT, Abdulkadri FR, Lawal B, Abdulfatah LB, Atolani O. An insight into the physicochemical, drug-likeness,

pharmacokinetics and toxicity profile of Kigelia africana (Lam) bioactive compounds. Al-Bahir. 2024;4(1):4. Doi:10.55810/2313-0083.1050

21. Selvaraj P, Ravindran CC, Balasubramaniam AK, Shankar PR, Thirunavukkarasu MB, Pushpanathan MS. Delivery and Developmental Strategies for Enhanced Blood–Brain Barrier Permeation—A Review. ChemistrySelect. 2025;10(47):e05570. Doi:10.1002/slct.202505570
22. Staneva Y, Iliev I, Georgieva S, Merdjanova A. In silico prediction of physicochemical properties and drug-likeness of omega-3 fatty acids. Ovidius University Annals of Chemistry. 2024;35(2):118-25. Doi: 10.2478/auoc-2024-0016
23. Qayed WS, Hassan MA, Şenol H, Taslimi P, Aboul-Fadl T. 2-Oxoindolin-thiazoline hybrids as scaffold-based therapeutics for T2DM-associated cognitive impairment: design, synthesis, in vitro and in silico studies. RSC Medicinal Chemistry. 2026;17, 317-342. Doi: 10.1039/D5MD00628G
24. Srivastava R. Theoretical studies on the molecular properties, toxicity, and biological efficacy of 21 new chemical entities. ACS omega. 2021;6(38):24891-901. Doi:10.1021/acsomega.1c03736
25. Choudhari S, Patil SK, Rathod S. Identification of hits as anti-obesity agents against human pancreatic lipase via docking, drug-likeness, in-silico ADME (T), pharmacophore, DFT, molecular dynamics, and MM/PB (GB) SA analysis. Journal of Biomolecular Structure and Dynamics. 2024;42(20):10688-710. Doi:0.1080/07391102.2023.2258407
26. Abbasi M, Mansourian M, Oskouie AA, Taheri S, Mahnam K. In-silico study MM/GBSA binding free energy and molecular dynamics simulation of some designed remdesivir derivatives as the inhibitory potential of SARS-CoV-2 main protease. Research in Pharmaceutical Sciences. 2024;19(1):29-41. Doi:10.4103/1735-5362.394818
27. Feldmann C, Yonchev D, Bajorath J. Analysis of biological screening compounds with single-or multi-target activity via diagnostic machine learning. Biomolecules. 2020;10(12):1605. Doi:10.3390/biom10121605